


# Competition between DivIVA and the nucleoid for ParA binding promotes segrosome separation and modulates mycobacterial cell elongation

Monika Pióro,<sup>1</sup> Tomasz Małecko,<sup>2</sup> Magda Portas,<sup>2</sup> Izabela Magierowska,<sup>2</sup> Damian Trojanowski,<sup>2</sup> David Sherratt,<sup>3</sup> Jolanta Zakrzewska-Czerwińska,<sup>1,2</sup> Katarzyna Ginda<sup>2,3†</sup> and Dagmara Jakimowicz <sup>1,2\*</sup>

<sup>1</sup>Laboratory of Molecular Biology of Microorganisms, Ludwik Hirsfeld Institute of Immunology and Experimental Therapy, Polish Academy of Sciences, Wrocław, Poland.

<sup>2</sup>Faculty of Biotechnology, Department of Molecular Microbiology, University of Wrocław, Wrocław, Poland.

<sup>3</sup>Department of Biochemistry, University of Oxford, Oxford, UK.

## Summary

Although mycobacteria are rod shaped and divide by simple binary fission, their cell cycle exhibits unusual features: unequal cell division producing daughter cells that elongate with different velocities, as well as asymmetric chromosome segregation and positioning throughout the cell cycle. As in other bacteria, mycobacterial chromosomes are segregated by pair of proteins, ParA and ParB. ParA is an ATPase that interacts with nucleoprotein ParB complexes – segrosomes and non-specifically binds the nucleoid. Uniquely in mycobacteria, ParA interacts with a polar protein DivIVA (Wag31), responsible for asymmetric cell elongation, however the biological role of this interaction remained unknown. We hypothesised that this interaction plays a critical role in coordinating chromosome segregation with cell elongation. Using a set of ParA mutants, we determined that disruption of ParA-DNA binding enhanced the interaction between ParA and DivIVA, indicating a competition between the nucleoid and DivIVA for ParA binding.

Having identified the ParA mutation that disrupts its recruitment to DivIVA, we found that it led to inefficient segrosomes separation and increased the cell elongation rate. Our results suggest that ParA modulates DivIVA activity. Thus, we demonstrate that the ParA-DivIVA interaction facilitates chromosome segregation and modulates cell elongation.

## Introduction

Cell cycle events must be coordinated; thus, bacterial cell elongation and its division need to be orchestrated with chromosome replication and segregation. Mycobacteria, the group of bacteria that encompasses pathogens with enormous impact on global health, i.e. *Mycobacterium tuberculosis*, as well as the saprophytic *Mycobacterium smegmatis*, exhibit unusual cell cycle features, including asymmetric cell elongation and chromosome segregation. Although the control of the mycobacterial cell cycle is crucial for pathogenicity, the orchestration of its key events remains unexplored.

While previous studies have described the main components of the mycobacterial chromosome segregation machinery, the ParA and ParB proteins, and have reported ParA interaction with a polar growth determinant DivIVA homologue (named Wag31 in mycobacteria) (Jakimowicz *et al.*, 2007; Ginda *et al.*, 2013; 2017; Uhía *et al.*, 2018), the exact mechanism of asymmetric chromosome segregation and the biological role of the ParA-DivIVA interaction have not been investigated. In mycobacteria, as in most studied bacterial species (*Bacillus subtilis*, *Caulobacter crescentus*, *Vibrio cholerae*, *Myxococcus xanthus*, *Corynebacterium glutamicum*, and *Streptomyces coelicolor*, but not *Escherichia coli* and some other  $\gamma$ -proteobacteria), origin of chromosomal replication (*oriC*) regions are organised into complexes named segrosomes by ParB binding to *oriC*-proximal *parS* sites (Chaudhuri and Dean, 2011; Wang *et al.*, 2013; Graham *et al.*, 2014; Zhang and Schumacher, 2017). Usually immediately (but in some species after some cohesion time) following the initiation of replication, ParB complexes

Accepted 9 October, 2018. \*For correspondence. E-mail dagmara.jakimowicz@uwr.edu.pl; Tel. +48 71 3752926; Fax +48 71 3757661.

<sup>†</sup>Current address: Oxford Nanoimaging, Wilkinson House, Jordan Hill Road, Oxford OX2 8DR, UK.

duplicate, and then one or both complexes are moved to their target cell locations. The separation of segrosomes and their movement are dependent on the action of ParA (Fogel and Waldor, 2006; Toro *et al.*, 2008; Gerdes *et al.*, 2010; Ptacin *et al.*, 2010; Lutkenhaus, 2012; Yamaichi *et al.*, 2012; Lim *et al.*, 2014); however, the generation of the force that moves segregating ParB complexes was under debate for a long time and only recently the widely accepted model emerged (Leonard *et al.*, 2005; Gerdes *et al.*, 2010; Lutkenhaus, 2012; Funnell, 2014; Lim *et al.*, 2014; Vecchiarelli *et al.*, 2014; Badrinarayanan *et al.*, 2015; Le Gall *et al.*, 2016; Surovtsev *et al.*, 2016). ParA homologues bind ATP, dimerise, and, as ATP-bound dimers, non-specifically interact with the nucleoid (Leonard *et al.*, 2005; Hester and Lutkenhaus, 2007). The first models of chromosome segregation suggested that dynamic ParA filaments were responsible for separation of ParB complexes (Ptacin *et al.*, 2010). According to diffusion-based models of ParB movement, ParA binding to nucleoid is crucial for the transport of ParB complexes. The interaction with the ParB complex enhances ATP hydrolysis and triggers ParA release from the nucleoid, generating a gradient of nucleoid-bound ParA and providing the driving force for segrosome movement (Lim *et al.*, 2014; Vecchiarelli *et al.*, 2014; Surovtsev *et al.*, 2016). Markedly, for most of the cell cycle, ParB complexes are precisely localised in bacterial cells in genus-specific positions, e.g. at the pole in *C. crescentus*, *V. cholerae* and *C. glutamicum*; subpolarly in *M. xanthus*; or midcell in vegetatively growing *B. subtilis* (Mohl and Gober, 1997; Harms *et al.*, 2013; Wang *et al.*, 2013; Kleckner *et al.*, 2014; Wang *et al.*, 2014; Badrinarayanan *et al.*, 2015; Bohm *et al.*, 2017). Interestingly, in *Mycobacterium* cells, the ParB complex is somewhat off-centred, and the mycobacterial chromosome segregation is partially asymmetric (Trojanowski *et al.*, 2015; Ginda *et al.*, 2017; Hołowka *et al.*, 2018). In mycobacteria, after segrosome duplication, both ParB complexes are moved towards opposite cell poles, but the complex that moves towards the new cell pole migrates faster and over a greater distance than the ParB complex moving towards the old cell pole (Ginda *et al.*, 2017). We hypothesised that the interaction between ParA and polarly localised DivIVA may be associated with the partial asymmetry of mycobacterial chromosome segregation (Ginda *et al.*, 2017).

Chromosome segregation and *oriC* positioning also depend on the interaction of chromosome segregation proteins with other protein complexes. A growing body of evidence shows that in various bacterial species (*C. crescentus*, *V. cholerae*, *C. glutamicum*, *S. coelicolor* and *M. xanthus*), the *oriC* region is anchored at the cell pole or subpolarly due to interactions between ParA or ParB and polar or subpolar proteins (Bowman *et al.*, 2008; Ebersbach *et al.*, 2008; Donovan *et al.*, 2012; Yamaichi *et al.*, 2012; Treuner-Lange and Søgaard-Andersen,

2014; Kois-Ostrowska *et al.*, 2016). In *C. crescentus*, the best-studied cell cycle model species, segregation proteins interact with the pole-associated proteins PopZ and TipN (Bowman *et al.*, 2008; Ebersbach *et al.*, 2008), while in *V. cholerae* polar HubP protein (Yamaichi *et al.*, 2012), controls the polar localisation of the *oriC* region. Similarly, in hyphal *S. coelicolor*, the interaction between ParA and a component of the polarisome complex, the Scy protein, is required for apical attachment of *oriC* (Ditkowski *et al.*, 2013; Kois-Ostrowska *et al.*, 2016). Interestingly, in *M. xanthus* ParA interaction with bactofilin scaffolds constrains the chromosome segregation machinery to the subpolar regions of the cell (Lin *et al.*, 2017). ParA and ParB proteins may also interact with a DNA replication protein DnaA in *B. subtilis* (Murray and Errington, 2008) and with a cell division protein MipZ in *C. crescentus* (Kiebusch *et al.*, 2012), which suggests that they coordinate chromosome segregation with chromosome replication and cell division, respectively. Thus, the interactions of chromosome segregation proteins play crucial, although not well understood, roles in the coordination of cell cycle events.

In *Mycobacterium*, ParA interacts with the coiled-coil DivIVA homologue (Ginda *et al.*, 2013). In Actinobacteria, DivIVA is essential for viability, and modifications of its level severely affect cell shape and morphology, reflecting its function in recruitment of the peptidoglycan synthesis machinery (Flärdh, 2003; Nguyen *et al.*, 2007; Flärdh, 2010; Letek *et al.*, 2012; Meniche *et al.*, 2014). As in other apically growing Actinobacteria, in mycobacteria, DivIVA localises predominantly at the cell poles, but interestingly, the protein is more abundant at the old pole than at the new pole (Kang *et al.*, 2008). That difference is correlated with the more efficient extension of the old pole than the new pole leading to asymmetric cell elongation, which is unique to mycobacteria (Aldridge *et al.*, 2012; Logsdon *et al.*, 2017). The maturation of the pole inherited from the mother cell influences the growth after cell division and the mycobacterial daughter cells differ in their growth rates. Additionally, cell division in mycobacteria is off-centred, generating daughter cells of uneven birth cell length (Joyce *et al.*, 2012; Santi *et al.*, 2013). Consistent with its function, DivIVA also localises at the nascent septa and, in fact, has been used as a marker of late cell division stages in *M. smegmatis* (Nguyen *et al.*, 2007; Kang *et al.*, 2008; Santi *et al.*, 2013; Ginda *et al.*, 2017). While DivIVA involvement in the anchorage of *oriC* has been shown in sporulating *B. subtilis* and in *C. glutamicum*, which is related to mycobacteria (Wu and Errington, 2003; Donovan *et al.*, 2012; Kloosterman *et al.*, 2016), the direct interaction between a DivIVA homologue and ParA seems to be unique to mycobacteria.

Here, we set out to explore the biological role of the ParA-DivIVA interaction in *M. smegmatis*. Since the

components of the chromosome replication, segregation, cell growth and division machinery are conserved between *M. smegmatis* and *M. tuberculosis*, the former may be used as a convenient model species for mycobacterial cell cycle studies. Using a set of ParA mutants, we investigated whether ParA dimerisation or DNA binding modulates its interaction with DivIVA. Having identified the mutation that abolished ParA recruitment to DivIVA, we examined its effects on key cell cycle processes – chromosome segregation, cell division and elongation.

## Results

### *ParA interaction with DivIVA is enhanced by disruption of ParA-DNA binding*

To explore how the ParA-DivIVA interaction contributes to chromosome segregation in *M. smegmatis*, we first asked whether the ParA dimerisation state or DNA binding influences the ParA interaction with DivIVA. The amino acid residues in the Walker A motif in ParA homologues that are required for their ATPase activity have been well described (Fung *et al.*, 2001; Yamaichi *et al.*, 2012; Ptacin *et al.*, 2014). Disruption of ATP binding is expected to inhibit ParA dimerisation and to consequently inhibit binding to the nucleoid, while the impairment of ATP hydrolysis was shown to stabilise the nucleoid-bound ParA dimer (Yamaichi *et al.*, 2012; Ptacin *et al.*, 2014). The nonspecific binding of ParA to DNA was shown to be determined by C-terminal arginines, and mutation of one of them was sufficient to abolish nucleoid binding (Hester and Lutkenhaus, 2007). Thus, we introduced mutations into *M. smegmatis* ParA that were expected to lead to disruption of ATP binding (K44A), hydrolysis (D68A) or DNA binding (R219E), and we established whether they affected ParA interactions with DivIVA in a heterologous *E. coli* system.

First, we confirmed that the mutations introduced into *M. smegmatis* ParA affected its interactions with DNA (Fig. S1A). While wild-type EGFP-ParA as well as EGFP-ParAD68A (dimeric) co-localised with the nucleoid in DAPI-stained *E. coli*, fluorescence of EGFP-ParAK44A (monomeric) and EGFP-ParAR219E (no DNA binding) was dispersed, which is consistent with the expected disruption of their interaction with DNA. Next, we tested if the mutations affected the ParA interaction with DivIVA in a bacterial two-hybrid (BTH) system using plate and quantitative assays (Fig. 1A, Fig. S1B). As observed previously (Ginda *et al.*, 2013), T18-DivIVA interacted with T25-ParA. Importantly, the level of mutated T25-ParA versions was the same as wild-type T25-ParA (Fig. S1D). Monomeric T25-ParAK44A did not interact with either T18-DivIVA or T18-ParB while the interaction of dimeric T25-ParAD68A with T18-DivIVA (and T18-ParB) was also

diminished, possibly due to enhanced interaction of ParA dimer with the nucleoid. Interestingly, non-DNA-binding T25-ParAR219E exhibited reduced binding to T18-ParB compared with wild-type ParA, while its interaction with T18-DivIVA was remarkably enhanced (Fig. 1A, Fig. S1B). This result suggested that disruption of ParA binding to DNA promoted its binding to DivIVA.

Thus, our observations suggested that ParA dimerisation is required for DivIVA binding. Moreover, they indicated competition between the nucleoid and DivIVA for ParA binding.

### *ParAT3A mutation disrupts the ParA interaction with DivIVA*

To determine the biological role of the interaction between ParA and DivIVA, we aimed to identify the amino acids in ParA engaged in the interaction. To this end, we constructed a BTH system library of T25-ParA\* mutants and screened it for the mutation in *parA* that impairs the interaction with T18-DivIVA.

The screening of the ParA mutant library identified an N-terminal threonine mutation (T3A) in ParA that inhibited its interaction with DivIVA (Fig. 1B, Fig. S1C). To confirm that the N-terminal fragment of ParA is indeed engaged in the interaction with T18-DivIVA, we used the N-terminally truncated mutant T25-ParA $\Delta$ 10aa (Fig. 1B, Fig. S1C). Moreover, the introduction of the same mutation into *M. tuberculosis* ParA (T25-ParA<sub>Mt</sub>TA) also abolished its interaction with its cognate DivIVA in BTH assays (Fig. S1F). Markedly, while T25-ParAT3A and T25-ParA $\Delta$ 10aa did not interact with T18-DivIVA, their dimerisation (interaction with T18-ParA) and interaction with T18-ParB were unaffected (Fig. 1B, Fig. S1C). However, the full co-localisation of EGFP-ParAT3A with a DAPI-stained *E. coli* nucleoid showed that the T3A mutation did not affect the ParA interaction with DNA (Fig. S1A). The disruption of the ParAT3A interaction with DivIVA was confirmed using co-localisation of EGFP-ParA and lcs-mCherry-DivIVA in *E. coli* (Ptacin *et al.*, 2014). In this system, the lcs protein fragment targeted the mCherry-DivIVA fusion protein, or mCherry in the control experiment, to the poles of *E. coli* cells and the influence of polar protein on EGFP-ParA localisation was tested. Wild-type EGFP-ParA was recruited to the poles by lcs-mCherry-DivIVA but not by lcs-mCherry (Fig. 1C). In the absence of DivIVA EGFP-ParA, fluorescence was extended along the cell. In contrast to wild-type EGFP-ParA, EGFP-ParAT3A did not localise to the poles in the presence of lcs-DivIVA-mCherry (and in the absence of DivIVA, in the negative control lcs-mCherry-producing cells), confirming the disruption of ParAT3A interactions with DivIVA (Fig. 1C).

Having established that the ParAT3A mutation disrupts the ParA-DivIVA interaction in heterologous *E. coli*

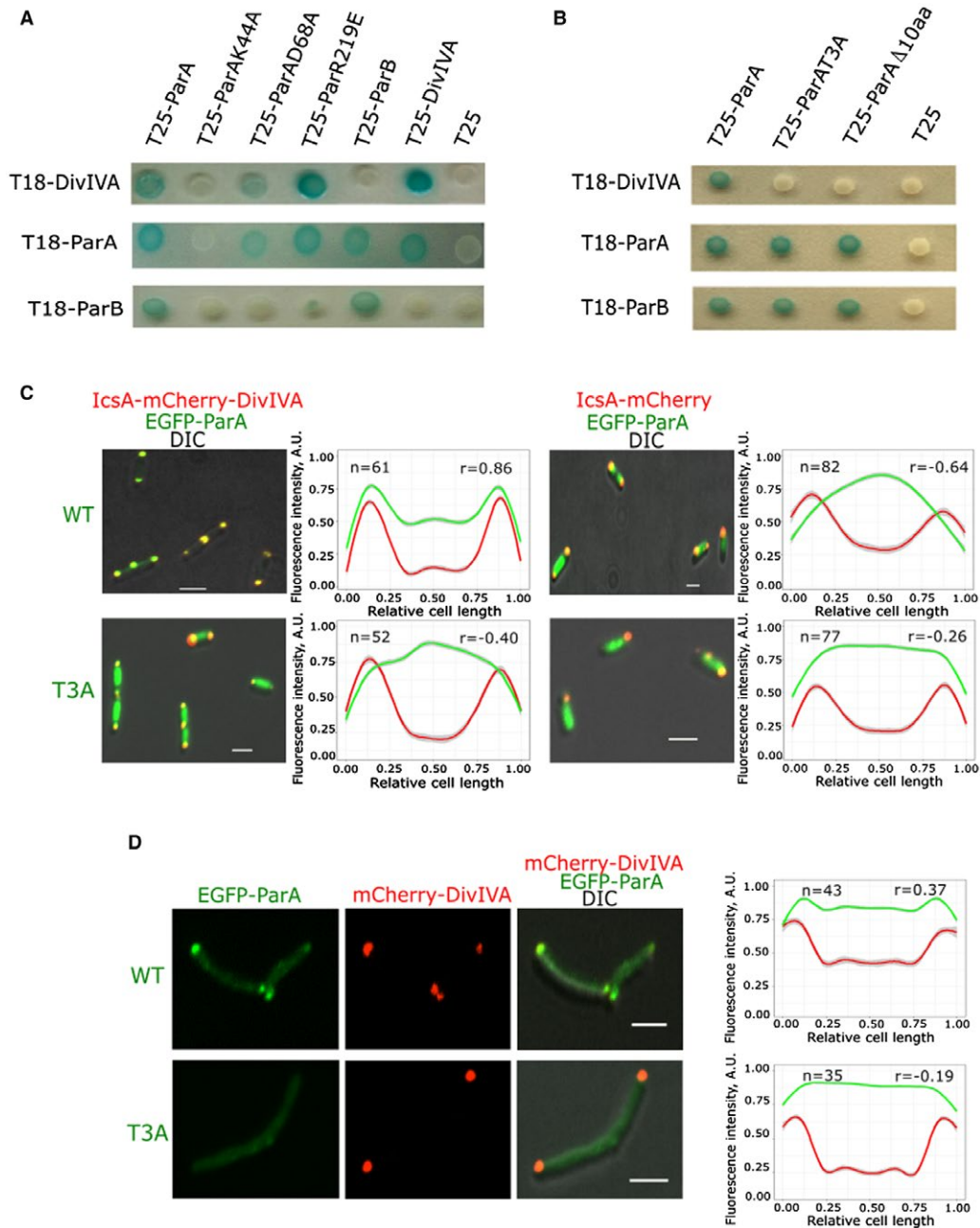


**Fig. 1.** Single amino acid mutations of ParA affect its interaction with DivIVA.

A. ParAK44A, ParAD68A and ParAR219E mutations affect ParA interactions with ParB and DivIVA in BTH assays. Images of example colonies of *E. coli* BTH101 cells co-producing T25 and T18 fusion proteins (as indicated) and grown on LB/X-gal/IPTG medium. The blue colour indicates an interaction between the fusion proteins.

B. ParAT3A mutation disrupts the ParA interaction with DivIVA in BTH assays. Top of each panel: colonies of *E. coli* BTH101 cells co-producing T25 and T18 fusion proteins (as indicated) and grown on LB/X-gal/IPTG medium. The blue colour indicates an interaction between the fusion proteins.

C. T3A mutation disrupts ParA co-localisation with mCherry-DivIVA in *E. coli*. Left panel: images of *E. coli* BL21 (DE3) cells producing EGFP-ParA or EGFP-ParAT3A (green) and IcsA-mCherry-DivIVA or IcsA-mCherry (negative control) (red fluorescence) merged with DIC images. Scale bar, 2  $\mu$ m. Right panel: green and red fluorescence intensity profiles along the cell length (50–80 cells of each strain were analysed, as indicated). Lines represent models fitted using a Loess algorithm implemented in the R program, and the grey area indicates 95% confidence intervals.

D. T3A mutation disrupts ParA co-localisation with mCherry-DivIVA in *M. smegmatis* cells. Example images of *M. smegmatis* cells producing DivIVA-mCherry (red) and EGFP-ParA (KG37 strain) or EGFP-ParAT3A (green), with both fluorescence signals merged with DIC (as indicated). Scale bar, 2  $\mu$ m. Right panel: green and red fluorescence intensity profiles, with their 95% confidence intervals along the cell length (35–43 cells analysed, as indicated). In C and D Pearson correlation coefficients 'r', as the measure of colocalisation, is indicated.

system, we set out to determine if this mutation also affects ParA localisation in *M. smegmatis* cells. To this end, we constructed an *M. smegmatis* strain that expressed *divIVA-mcherry* (under its native promoter, as an additional *divIVA* copy) and *egfp-parAT3A* (under its native promoter, instead of wild-type *parA*) and compared the localisation of both fusion proteins to the previously described localisation of *divIVA-mcherry* and *egfp-parA*

(Ginda *et al.*, 2013). Importantly, we previously observed that microscopic specimen preparation method affected the localisation of EGFP-ParA in *M. smegmatis* and while in live cells analysed at optimal conditions EGFP-ParA fluorescence stretched from the pole towards the centre of the cell (Ginda *et al.*, 2017), the procedure that involved the short drying of the cells on slides promoted the polar localisation of ParA (Ginda *et al.*, 2013). Here, using the

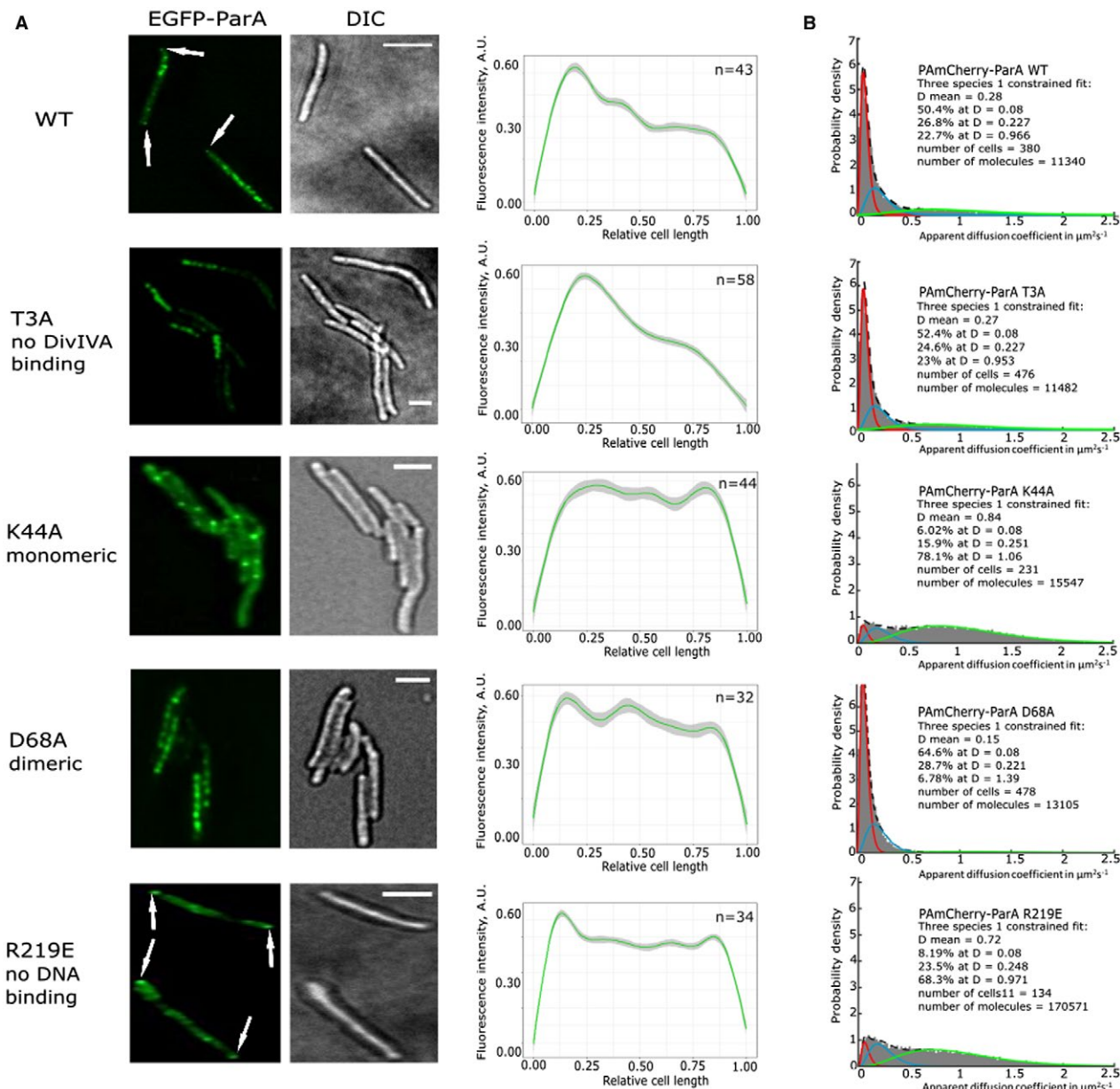


**Fig. 2.** Disruption of ATP or DNA binding by ParA affects its localisation and mobility in *M. smegmatis* cells.

**A.** SIM analysis showing altered localisation of mutant EGFP-ParA in *M. smegmatis* cells under optimal growth conditions. Left panel: example SIM images showing the fluorescence of EGFP-ParA (green) and *M. smegmatis* cells in transmitted light (DIC), as indicated. The white arrows mark the faint fluorescence focus on the cell pole. Right panel: relative EGFP fluorescence intensity (the maximum value of fluorescence set at 1) measured along the cell length in SIM images; 32–58 cells were analysed, as indicated.

**B.** PALM analysis showing influence of ParA mutations on its dynamics. Distributions of the apparent diffusion coefficient,  $D^*$ , of single-molecule trajectories of wild-type and mutant PAmCherry-ParA molecules (the number of cells and protein molecules analysed for each mutant are indicated). Insets show the fractions of PAmCherry-ParA with a diffusion coefficient in a particular range.

latter conditions, we observed that while wild-type ParA co-localised with DivIVA at the poles, EGFP-ParAT3A fluorescence was more dispersed and did not overlap with DivIVA-mCherry fluorescence (Fig. 1D). This analysis confirmed that the ParAT3A mutation eliminated its co-localisation with DivIVA *in vivo* in *M. smegmatis* cells.

To summarise, we established that single amino acid mutation (T3A) in *M. smegmatis* (and *M. tuberculosis*) ParA was sufficient to disrupt its interaction with DivIVA in *E. coli* systems and in *M. smegmatis* cells. Moreover, we showed that the T3A mutation in ParA did not affect dimerisation or the ParA interactions with ParB and the nucleoid.

#### *Abolished ParA recruitment to DivIVA slightly affects ParA localisation in M. smegmatis cells*

Next, we checked if the disruption of the ParA interaction with DivIVA influences its behaviour under optimal growth conditions in *M. smegmatis* cells. To this end, we used a strain in which the *egfp-parAT3A* or *PAmcherry-parAT3A* gene complemented the *parA* deletion as compared to *parA* deletion complemented with the wild-type *egfp-parA* (Ginda *et al.*, 2013) or *PAmcherry-parA* (Fig. S3). Time-lapse epifluorescence microscopy and high-resolution structured illumination microscopy (SIM) were used to localise EGFP-ParAT3A. Additionally, we analysed the mobility of PAmCherry-ParA and PAmCherry-ParAT3A using single molecule tracking with application of photoactivated localisation microscopy (PALM).

Analysis of the EGFP-ParAT3A dynamics using time-lapse fluorescence microscopy did not indicate distinct differences in the pattern of localisation, apart from the lack of a polar ParA complex, which was transiently visible in the majority of the cells with wild-type ParA (72% of 141 analysed cells) (Fig. S2A, B, C; Movies S1 and S2). The SIM analysis confirmed that under optimal conditions, the localisation of EGFP-ParAT3A was similar to that of the wild-type EGFP-ParA. The fluorescence of wild-type EGFP-ParA extended from one cell pole towards midcell, with its intensity gradually decreasing away from the cell pole, while a second, less intense ParA focus was visible at the other pole in most of the cells (Fig. 2A). The EGFP-ParAT3A fluorescence was still restricted to half of the cell, but its maximum intensity (the brightest pixel localisation) was slightly shifted away from the pole, and the focus at the other pole was absent.

PALM analysis showed that the T3A mutation did not affect the mobility of ParA (Fig. 2B). The average diffusion coefficient of the wild-type PAmCherry-ParA was  $0.28 \mu\text{m}^2 \text{s}^{-1}$ ; 50% of the molecules were immobile (diffusion coefficient below  $0.08 \mu\text{m}^2 \text{s}^{-1}$ ), suggesting that they were bound to the nucleoid, and 23% of the molecules had diffusion coefficients above  $0.966 \mu\text{m}^2 \text{s}^{-1}$ . The average

diffusion coefficient of PAmCherry-ParAT3A was  $0.27 \mu\text{m}^2 \text{s}^{-1}$ , which was almost identical to that of the wild-type protein PAmCherry-ParA, and the fractions of mobile and immobile molecules were highly similar.

Thus, the localisation and mobility of ParA in *M. smegmatis* were only slightly affected by the T3A mutation.

#### *Binding to nucleoid regulates ParA mobility, affecting its interaction with DivIVA in M. smegmatis cells*

Having established that ParA binding with DNA modulates protein interaction with DivIVA in an *E. coli* heterologous system, we examined whether ParA mutations that affect its interaction with DNA influence its recruitment to DivIVA in *M. smegmatis* cells. To this end, we constructed a set of *M. smegmatis* mutant strains in which the *parA* deletion was complemented by *parAD68A*, *parAK44A* or *parAR219E* genes N-terminally fused with a fluorescent protein gene, either *egfp* or *PAmcherry* and compared them to the strains complemented with the wild-type *egfp-parA* (Ginda *et al.*, 2013) or *PAmcherry-parA* (Fig. S3, Supplementary Table 1). We analysed ParA localisation, particularly the formation of a polar focus and mobility using epifluorescence microscopy, SIM and PALM.

The epifluorescence microscopy and SIM analysis revealed that the localisation of non-DNA-binding and dimeric ParA was severely affected (Fig. 2A and Fig. S4). The dimeric EGFP-ParAD68A was visible as clustered foci, resembling the pattern of nucleoid staining (Hołowka *et al.*, 2017), which reflected its enhanced DNA binding. Monomeric EGFP-ParAK44A was more dispersed along the cell length, with occasional randomly positioned bright foci (presumably accumulations of nonfunctional protein), which is in agreement with its abolished DNA binding. Similarly, the fluorescence of non-DNA-binding EGFP-ParAR219E was more diffuse than of wild-type EGFP-ParA; however, in contrast to the monomeric and dimeric versions, it formed brighter foci at the poles (Fig. 2A and Fig. S4). The enhanced polar localisation of the non-DNA-binding mutant of ParA was presumably the result of its enhanced interaction with DivIVA.

Finally, we used PALM analysis to confirm that the mutations that abolished binding and the hydrolysis of ATP affect PAmCherry-ParA mobility (Fig. 2B). The monomeric ParA K44A showed significantly increased mobility (average diffusion coefficient  $0.84 \mu\text{m}^2 \text{s}^{-1}$  compared to  $0.28 \mu\text{m}^2 \text{s}^{-1}$  for wild-type ParA), while the dimeric ParAD68A had decreased mobility (average diffusion coefficient  $0.15 \mu\text{m}^2 \text{s}^{-1}$ ). These results are consistent with the idea that the elimination of ATP binding by the K44A mutation inhibits ParA interaction with the nucleoid, while the inhibition of ATP hydrolysis by the D68A mutation prevents ParA diffusion from DNA. The non-DNA-binding ParAR219E showed substantially increased mobility (average

diffusion coefficient  $0.72 \mu\text{m}^2 \text{s}^{-1}$ ). Notably, the fraction of highly mobile molecules (diffusion coefficient above  $1.06 \mu\text{m}^2 \text{s}^{-1}$ ) was 68% for non-DNA-binding ParAR219E and 78% for monomeric ParAK44A. This difference (10% of molecules) probably resulted from ParAR219E interacting with DivIVA, as suggested by the polar localisation of EGFP-ParAR219E.

Thus, our analysis showed that ParA mobility and localisation were highly affected by its interaction with the nucleoid. The enhanced polar localisation of the ParA mutant with abolished DNA binding reinforces the idea of competition between the polar DivIVA complex and the nucleoid for ParA binding.

*Disruption of the ParA interaction with DivIVA affects chromosome segregation to a lesser extent than modified binding to the nucleoid*

Having observed that the mutation of ParA that disrupted its interaction with DivIVA only slightly affected its localisation, we wondered whether this mutation affects *M. smegmatis* chromosome segregation. To compare the effect of eliminating the interaction with DivIVA with the consequences of disrupting the other ParA interactions (DNA binding, dimerisation), we analysed chromosome segregation in the above-described *M. smegmatis* strains in which the *parA* deletion was complemented by the *egfp-parAT3A*, *egfp-parAD68A*, *egfp-parAK44A* and *egfp-parAR219E* genes or wild-type *egfp-parA*.

Since chromosome segregation defects lead to the formation of anucleate cells, which is also reflected in growth rates, we first compared the growth of the *M. smegmatis* strains producing mutated ParA instead of the wild-type protein (Fig. 3A). As expected, the presence of monomeric ParAK44A resulted in culture growth inhibition similar to that observed for *parA* deletion. Additionally, the production of dimeric ParAD68A slowed the growth, but to a lesser extent, while the presence of non-DNA-binding ParAR219E impaired culture growth more than the *parA* deletion. Markedly, the growth of the strain with ParAT3A was similar to the growth of the control strain or even somewhat faster. Thus, the disruption of the ParA-DivIVA interaction had no visible effect on *M. smegmatis* growth under optimal conditions.

Next, we microscopically analysed the DNA-stained cells of mutant strains to evaluate the fraction of anucleate cells and the average cell length, which had previously been reported to be affected by *parA* deletion (Ginda et al., 2013). Abolished ParAT3A recruitment to DivIVA led to modest disturbances of chromosome segregation (7% anucleate cells) (Fig. 3A, inset). In contrast, the production of monomeric ParAK44A led to severe segregation defects (19% anucleate cells) similar to those resulting from *parA* deletion (23% anucleate cells). Accordingly,

dimeric ParAD68A and non-DNA-binding ParAR219E also caused aberrant chromosome segregation (16 and 17% anucleate cells respectively). The obtained results are in agreement with the culture growth analysis and with the predicted roles of ParA ATP binding, hydrolysis and DNA interaction in the segregation of ParB complexes.

A comparison of cell lengths (only nucleate cells were used in the analysis; anucleate minicells were excluded) revealed that the abolished DivIVA interaction with ParAT3A led to a slight decrease in cell length (median  $3.2 \mu\text{m}$ ) from its value for wild-type cells (median  $3.4 \mu\text{m}$ ) and  $\Delta parA$  cells (median  $3.7 \mu\text{m}$ ), while the dimeric ParAD68A and monomeric ParAK44A led to the formation of cells longer than wild-type cells ( $4.1$  and  $3.7 \mu\text{m}$  respectively), and the non-DNA-binding ParAR219E significantly increased the average cell length (median  $5.1 \mu\text{m}$ ) (Fig. 3B).

Thus, the elimination of the ParA interaction with DivIVA did not have as profound an effect on chromosome segregation as the disruption of ATPase activity or DNA binding.

*Disruption of the ParA interaction with DivIVA diminishes the efficiency of segrosome separation*

Although the ParA3TA mutation did not significantly increase the number of anucleate cells, we wanted to know whether abolishing the DivIVA-ParA interaction influenced the rapid movement of the newly duplicated ParB complexes immediately after the initiation of chromosome replication (Trojanowski et al., 2015; Ginda et al., 2017). To this end, we introduced the *parAT3A* gene (complementing the *parA* deletion) into a strain with marked segrosomes (*parB-mNeon*) and replisomes (*dnaN-mCherry*) (Trojanowski et al., 2015), and using time-lapse fluorescence microscopy, we analysed the positions of ParB-mNeon complexes after the initiation of chromosome replication, marked by the appearance of a DnaN-mCherry focus. As reported earlier (Trojanowski et al., 2015; Ginda et al., 2017), in the control strain, the duplicated ParB-mNeon complexes separated to opposite cell halves soon after the initiation of replication. The movement of ParB was not as rapid as reported earlier, probably due to the differences in genetic background (*parA* gene N-terminally fused to fluorescent protein gene used to complement the *parA* deletion). Notably, the abolished ParA3TA binding to DivIVA impaired the efficient separation of the ParB complexes. In the ParAT3A strain, as in the control strain, the ParB complex that was transferred towards the new pole exhibited higher velocity than the one moving towards the old pole; however, its movement was more uniform over time, and the ParB complex reached its final position later than in the control strain (wild-type ParA) (Fig. 3C, D). Interestingly, the positioning of the old pole ParB complex was also

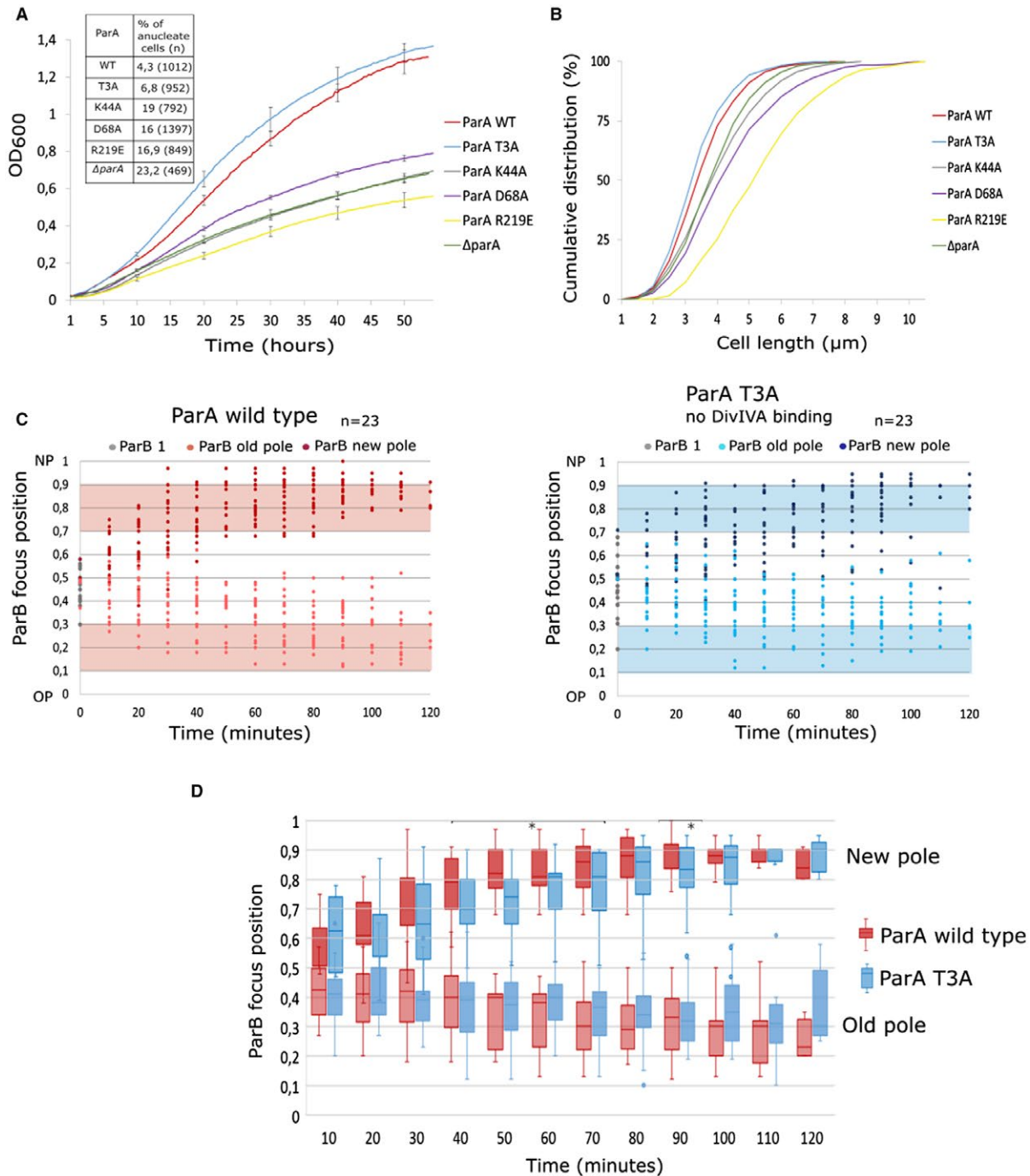


**Fig. 3.** ParA3TA mutation marginally affects growth and chromosome segregation but impairs segrosome separation.

A. Culture growth rate and chromosome segregation are affected by ParAK44A, ParAD68A and ParAR219E to a greater extent than by ParAT3A. Growth curves of strains carrying ParAT3A, ParAK44A, ParAD68A and ParAR219E mutations, obtained using a Bioscreen C instrument. The results are the average of three independent experiments; bars indicate standard errors. Inset: the percentage of anucleate cells identified in the images of the DAPI-stained cells of analysed strains (the number of cells analysed, *n*, is indicated).

B. ParAT3A, ParAK44A, ParAD68A and ParAR219E mutations affect cell length. Cumulative distribution showing the percentage of cells with a particular length, measured in the microscope images of DAPI-stained cells (the number of cells analysed, *n*, is indicated).

C. ParA3TA mutation disturbs ParB-mNeon focus positioning. The distance between ParB-mNeon focus position and the cell pole was measured during the cell cycle in the control strain (left panel) and in the strain carrying the ParAT3A mutation (right panel). The initiation of replication (time 0) was set as the appearance of a DnaN-mCherry focus (23 cells analysed).

D. Comparison of the position of the old pole (left panel) and the new pole (right panel) ParB-mNeon focus position in time. Crossbars show the mean with 95% confidence intervals. Statistically significant ( $p < 0.05$ , *T*-student test) difference in positioning of the ParB-mNeon complexes is marked with asterisks.

somewhat affected, and it showed the greater variation in ParA3TA strain than in the control strain (Fig. 3C, D).

Since the old pole segrosome was shown to be located close to the edge of the nucleoid (Hołowka *et al.*, 2018), the observation that ParA interaction with DivIVA was required for the efficient separation and positioning of ParB complexes suggests that it may affect the positioning of the nucleoid in relation to the cell pole. To confirm this notion, we measured the distance between the nucleoid and the pole of the cell farther away from DNA (the old pole, as suggested by previous studies [Hołowka *et al.*, 2018]) in DAPI-stained cells of the control strain (*parA* deletion complemented by *egfp-parA*) and the ParA3TA strain (*parA* deletion complemented by *egfp-parAT3A*). Indeed, the edge of the nucleoid was somewhat more shifted away from the pole in the strain carrying the ParA3TA mutation than in the control strain (median 27% of cell length in the ParA3TA strain and 21% in the control strain, *p* value < 0.0001) (Fig. S5).

To sum up, the elimination of the ParA interaction with DivIVA, although did not have a profound effect on chromosome segregation, affected the efficient separation of segrosomes. Our results suggest that the ParA interaction with DivIVA may contribute to positioning of ParB complexes and the whole nucleoid in relation to the old cell pole.

#### *The interaction between ParA and DivIVA influences the cell elongation rate*

Due to the observed slight increase in growth rate and decrease in cell length resulting from the ParAT3A mutation, in the course of exploring the effects of disrupting the ParA-DivIVA interaction, we decided to elucidate the influence of the ParAT3A mutation on the cell cycle. To this end, we used time-lapse microscopy and cell membrane staining to visualise cell division and to compare the cell length increment ( $\Delta l$ ) and the time between cell divisions and cell elongation rate ( $\Delta l/t$ ) in the control strain (*parA* deletion complemented by *egfp-parA*) and in the strain carrying the ParAT3A mutation (*parA* deletion complemented by *egfp-parAT3A*) (Fig. 4A). Since the mycobacterial daughter cells differ in growth rate depending on the maturation of the pole inherited from the mother cell, we analysed the cell cycles of both daughter cells independently.

A time-lapse analysis revealed that the disrupted ParA3TA interaction with DivIVA increased the cell elongation rate and shortened the interdivision time (Fig. 4B and C, Movies S1 and S2). The elongation rate of the control strain cells was  $0.79 \pm 0.09$  and  $0.65 \pm 0.17 \mu\text{m h}^{-1}$  for old pole- and new pole-inheriting cells respectively. The measured cell cycle parameters of the control strain differed from earlier reports (Trojanowski *et al.*, 2017),

plausibly due to the differences in genetic background of the analysed strains and conditions of the microscopy experiment, such as exposure time. The ParA3TA mutation significantly ( $p < 0.001$ ) increased the cell extension rate to  $1.08 \pm 0.18$  and  $0.82 \pm 0.25 \mu\text{m h}^{-1}$  for old pole- and new pole-inheriting cells, respectively. While the control strain old pole-inheriting cells divided every  $198 \pm 37$  min and new pole-inheriting cells every  $192 \pm 23$  min, the ParAT3A mutation resulted in shortening the interdivision time to  $161 \pm 26$  and  $168 \pm 24$  min for old pole- and new pole-inheriting cells, respectively. However, we did not observe a change in cell length increment between cell division events ( $\Delta l$ ), which was very similar for both daughter cells in the control and mutant strains (Fig. 4D). Thus, faster cell elongation was associated with shorter interdivision time, as expected because of observed slight decrease in the cell length.

Since non-DNA-binding ParAR219E showed enhanced recruitment to DivIVA (indicated by BTH studies and its localisation in *M. smegmatis*), we decided to check whether this ParA mutation also affected the cell extension rate (in the strain with *egfp-parAR219E* complementing the *parA* deletion). The ParAR219E mutation led to the formation of a high fraction of anucleate minicells, similar to that observed in the *parA* deletion strain, and an increase in the average cell length (Fig. 4A and B). Time-lapse analysis revealed that the anucleate minicells usually formed at the new pole of the cell (Fig. S2D), indicating that the elimination of ParA binding to the nucleoid disturbed the transfer of the ParB complex towards the new pole. Due to the formation of anucleate cells, we analysed the extension rate of the daughter cells that inherited the older mother cell pole. Surprisingly, the presence of non-DNA-binding ParAR219E elevated the cell extension rate ( $1.01 \pm 0.24 \mu\text{m h}^{-1}$ ) compared to the control strain ( $0.79 \pm 0.09 \mu\text{m h}^{-1}$ ) (Fig. 4B). The ParAR219E mutation, similarly to ParAT3A, also shortened the interdivision time to  $142 \pm 28$  min from its control strain value ( $192 \pm 23$  min) (Fig. 4C). This difference showed that the enhanced interaction between ParA and DivIVA also affected the cell elongation rate, albeit in a manner that was surprisingly similar to the lack of interaction between ParA and DivIVA.

In summary, the alteration of the ParA-DivIVA interaction affected the cell cycle. Surprisingly, both the enhancement and elimination of the ParA interaction with a polar protein increased the cell elongation rate and shortened the division time.

## Discussion

The interaction between ParA and the polar growth determinant DivIVA is unique to *Mycobacterium* (Ginda

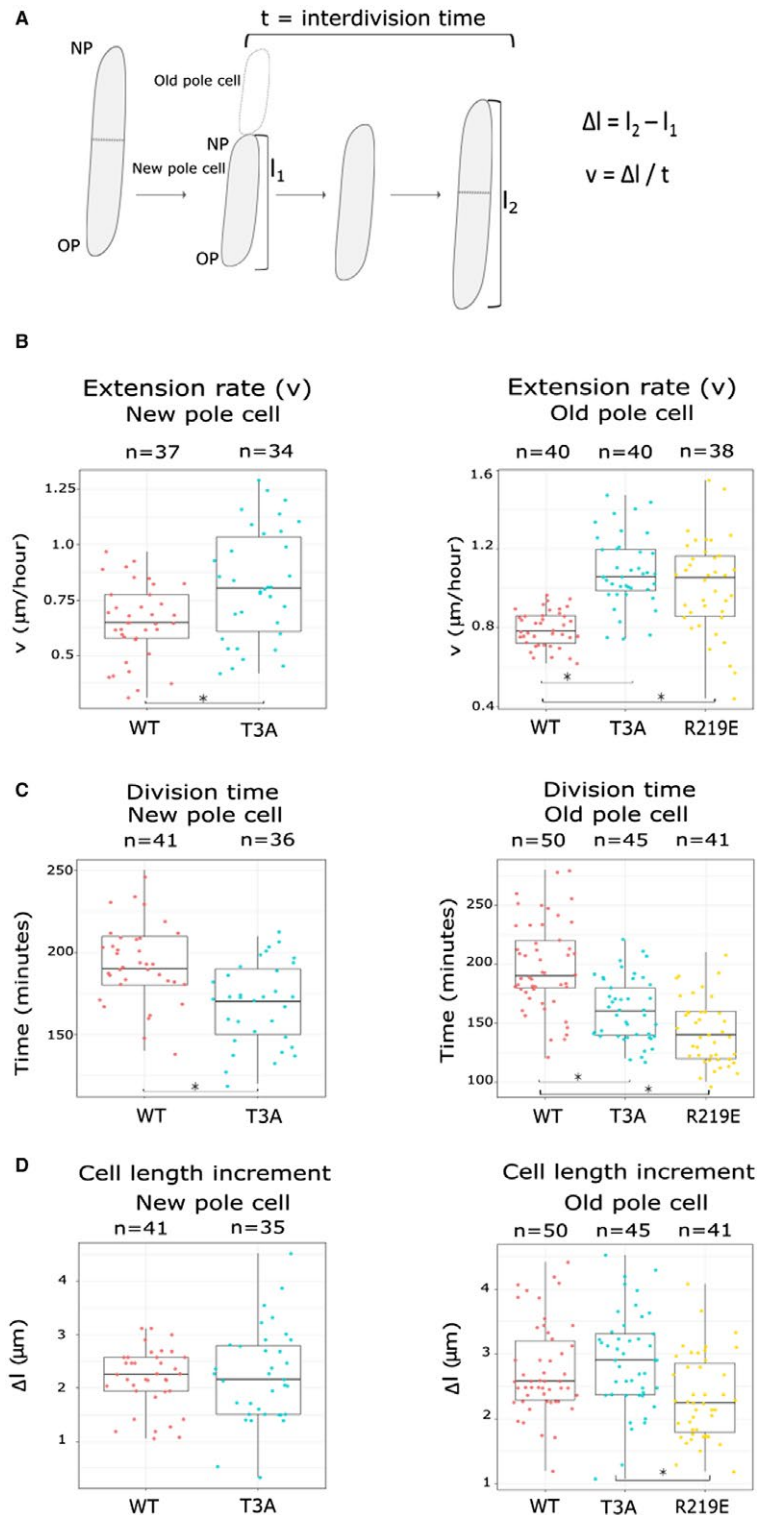


**Fig. 4.** Modulation of the ParA-DivIVA interaction affects the cell cycle, increasing the cell elongation rate and decreasing the interdivision time. A. Scheme of the cell cycle showing the measured parameters: cell elongation rate ( $v$ ), interdivision time ( $t$ ) and interdivision cell length increment.

B-D. The cell elongation rate (B), interdivision time (C) and cell length increment (D) are altered in the ParAT3A and ParAR219E strains from their values in the control strain (wt). The cell cycle parameters were analysed for a new pole- (left panel) and an old pole-inheriting (right panel) cell. The boxplot shows the median (line), first and third quartiles (lower and upper 'hinges'), and coloured points indicate all observations. The number of analysed cells ( $n$ ) varied between 30 and 50, as indicated. The statistically significant differences ( $p < 0.001$ ) are marked with asterisks.

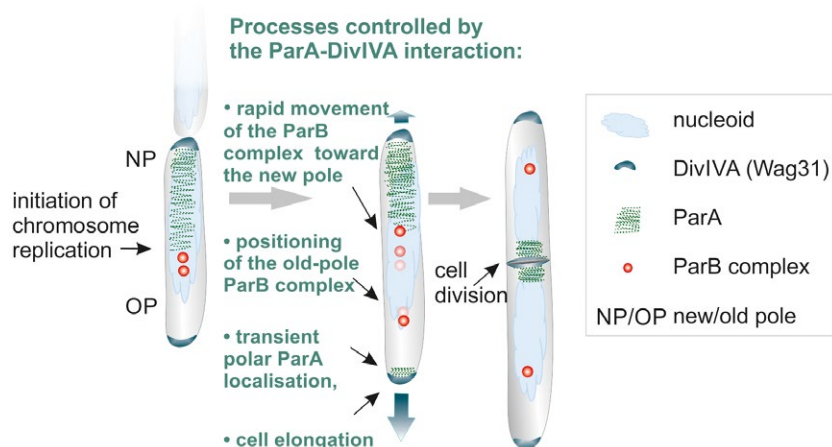


**Fig. 5.** Model of the *M. smegmatis* cell cycle showing suggested roles of the ParA-DivIVA interaction. DivIVA-ParA interaction facilitates segrosome separation, controls positioning of the *oriC* and modulates cell elongation affecting interdivision time.

*et al.*, 2013). We hypothesised that it may be a prerequisite for the unusual cell cycle of mycobacteria, which involves uneven polar cell extension resulting from the faster growth of the old pole and partially asymmetric chromosome positioning and segregation (Aldridge *et al.*, 2012; Santi *et al.*, 2013; Singh *et al.*, 2013; Ginda *et al.*, 2017; Hołowka *et al.*, 2018). The application of ParA mutations that affect the ATP binding, hydrolysis or DNA binding (Leonard *et al.*, 2005; Hester and Lutkenhaus, 2007) allowed us to examine how the ParA-DivIVA interaction is linked to ParA-mediated chromosome segregation. The identification of a ParA mutation that abolishes the ParA-DivIVA interaction revealed the biological significance of the ParA-DivIVA interaction.

#### Competition between the nucleoid and DivIVA for ParA binding

Our studies revealed a competition between the nucleoid and DivIVA for ParA binding. The finding that impaired DNA binding promotes ParA recruitment to DivIVA is consistent with an earlier observation that in anucleate minicells (such as produced by the  $\Delta parB$  strain) EGFP-ParA localises to the old cell pole (Ginda *et al.*, 2017). In contrast, a stable ParA dimer with enhanced DNA binding (ParAD68A) shows decreased interaction with DivIVA. Thus, we conclude that the interaction with DivIVA occurs when ParA is released from the nucleoid.

The interaction between DivIVA and ParA released from the nucleoid is only somewhat reminiscent of the recruitment of ParA by PopZ in phylogenetically distant *C. crescentus*. Interaction with PopZ and TipN with ParA dimer was enhanced by disrupting the ParA interaction with DNA and was inhibited by abolishing ParA ATP hydrolysis (Schofield *et al.*, 2010; Ptacin *et al.*, 2014), similar to the observations of the ParA interaction with

DivIVA in *M. smegmatis*. However, in *C. crescentus* the ATP-bound ParA monomer showed enhanced interaction with polar protein, while preliminary studies of *M. smegmatis* ParAG40V indicated its diminished interaction with DivIVA (Fig. S1E). We hypothesise that the mycobacterial DivIVA-ParA interaction may also be important for *oriC* positioning in cell; however, due to their asymmetric cell elongation, mycobacteria might have developed a unique mechanism controlling of the *oriC* localisation.

#### Role of the ParA-DivIVA interaction in chromosome segregation

The identification of an N-terminal threonine in ParA required for the interaction with DivIVA allowed us to explore the consequences of disrupting that interaction (ParAT3A mutation). We expected that disruption of the ParA-DivIVA interaction would severely affect ParA behaviour and chromosome segregation. Surprisingly, the disruption of binding to DivIVA only marginally influenced ParA localisation and did not affect ParA mobility, which appeared to be mostly dependent on the interaction with the nucleoid. Moreover, it did not significantly increase the number of anucleate cells, in striking contrast to the effects of other ParA mutations (R219E, K44A and D68A). This observation indicates that, in contrast to ParA interactions with polar proteins in *C. crescentus*, its interaction with DivIVA does not critically contribute to ParA relocation under optimal conditions.

A careful analysis of ParB positioning during the cell cycle revealed that the disruption of the ParA interaction with DivIVA altered the movement of segrosomes. It was previously shown that the ParB complex that migrates towards the new cell pole exhibits higher velocity than the one migrating towards the old cell pole (Ginda *et al.*, 2017; Uhía *et al.*, 2018). Moreover, a recent visualisation of the

nucleoid in relation to the localisation of ParB complexes revealed that the nucleoid is asymmetrically positioned and shifted towards the new pole and that the old pole segrosome is located close to the edge of the nucleoid throughout most of the cell cycle (Hołowka *et al.*, 2018). Thus, the ParB complex that is segregated towards the new pole migrates over the whole nucleoid length, and we can conclude that its movement is dependent on the ParA association with the nucleoid (Fig. 5). As in *V. cholerae* and *C. crescentus*, the movement of this ParB complex is accompanied by ParA fluorescence extending and shrinking towards the new pole (Fogel and Waldor, 2006; Toro *et al.*, 2008; Ginda *et al.*, 2017). The polar sequestration of ParA in *C. crescentus* was suggested to prevent reassembly of ParA at the nucleoid (Schofield *et al.*, 2010; Ptacin *et al.*, 2014). We suggest that in *M. smegmatis* recruitment of ParA to DivIVA would play similar role. In the *M. smegmatis* strain with a disrupted ParA-DivIVA interaction, the migration of the ParB complex towards the new pole slowed down, suggesting that interaction with DivIVA facilitates the formation of the ParA gradient over DNA, which fuels the migration of the ParB complex. In the absence of the ParA-DivIVA interaction, the localisation of the ParA cloud was slightly shifted away from the pole. Notably, the precise positioning of the old pole ParB complex was also somewhat affected by the disruption of ParA interaction with DNA. Since ParA was associated with DivIVA at the old pole (in the nucleoid-free region), it is tempting to suggest that ParA interacting with DivIVA, instead of the ParA gradient over the nucleoid, is responsible for positioning of the ParB complex at a certain distance from the old cell pole. This idea is supported by the observation that the ParAR219E mutation (which abolishes DNA binding) leads to the formation of anucleate cells at the new cell pole, indicating that the *oriC* positioning at the old cell pole is intact in these cells and not dependent on ParA-DNA interaction, but may be somehow dependent on ParA-DivIVA interaction. Notably, our earlier studies showed that in  $\Delta parA$  strain old pole ParB complex was often shifted towards the pole, which might indicate the rearrangement of polar interactions in absence of ParA (Ginda *et al.*, 2017). Thus, the segregation of two ParB complexes in mycobacterial cells, although apparently bidirectional, is presumably dependent on two different mechanisms, which would explain the difference in their translocation.

Considering that mycobacterial cells elongate mainly at the old cell pole, the interaction between DivIVA and ParA might play a role in the positioning of the nucleoid behind the extending pole, similar to the interaction between ParA and the polar coiled-coil protein Scy in hyphal *Streptomyces*, which, as a mycobacterium, belongs to Actinobacteria. In *S. coelicolor*, ParA, due to its interaction with a polar complex, anchors the *oriC* of

the apical chromosome at the hyphal tip and maintains its constant distance to the tip (Kois-Ostrowska *et al.*, 2016). Considering the distance between the nucleoid and DivIVA complex at the pole, it is likely that other, additional protein(s) takes part in the ParB-*oriC* positioning at a specific distance from the old pole in *M. smegmatis*, similarly as in *M. xanthus* (Lin *et al.*, 2017).

#### Function of ParA in the regulation of DivIVA activity

The vital question that we addressed is how the interaction with ParA affects DivIVA function. Remarkably, we found that the ParA mutation that disrupts its interaction with DivIVA affects the cell elongation rate. In all analysed strains, the increase in the elongation rate is accompanied by shortening of the interdivision time, and the cell length increment between cell divisions is constant, which is in agreement with the 'adder' mode of growth suggested for mycobacteria (Aldridge *et al.*, 2012; Santi *et al.*, 2013; Kieser and Rubin, 2014; Logsdon *et al.*, 2017; Priestman *et al.*, 2017). The elongation of mycobacterial cells is dependent on the activity of DivIVA, which recruits the peptidoglycan synthesis complex (Meniche *et al.*, 2014). The activity and abundance of DivIVA are correlated with the pole maturation, and the daughter cells that inherit the old pole elongate faster than their siblings that inherit the new pole (Kang *et al.*, 2008; Aldridge *et al.*, 2012; Singh *et al.*, 2013; Kieser and Rubin, 2014; Logsdon *et al.*, 2017). Interestingly, the DivIVA homologue in *M. tuberculosis* is phosphorylated, and the phosphorylated protein is more abundant during exponential growth, suggesting it is more efficient at stimulating peptidoglycan biosynthesis (Kang *et al.*, 2005; Jani *et al.*, 2010). DivIVA activity is also regulated by interactions with its partner proteins, for example, cell wall synthesis protein A (CwsA) and LamA, the protein that is responsible for the switch between cell division and elongation (Plocinski *et al.*, 2012; Plocinski *et al.*, 2013; Rego *et al.*, 2017). The interplay between DivIVA and LamA may contribute to the reorganisation of the polar elongation complex. Thus, to control cell elongation, ParA may affect DivIVA stability, its phosphorylation status or its interaction with other proteins. Interestingly, an influence of ParA on cell elongation has also been observed in other Actinobacteria. In *C. glutamicum*, in the absence of ParA, the cell length was reduced, indicating that the interaction between the ParB-*oriC* complex and polar proteins controls apical growth, but the exact mechanism of this phenomenon has not been described (Donovan *et al.*, 2013; Donovan and Bramkamp, 2014). In *S. coelicolor*, ParA accumulation inhibits cell extension, indicating that ParA controls hyphal elongation during sporulation. ParA interaction with apical Scy was suggested to provide the switch

between cell elongation and cell division (Ditkowski *et al.*, 2013; Donczew *et al.*, 2016). We speculate that the ParA-DivIVA interaction in mycobacteria might be a similar checkpoint.

Surprisingly, disruption of the ParA interaction with DivIVA and elimination of its binding to DNA, which enhances recruitment to DivIVA, similarly increased the cell elongation rate and decreased the division time. On the one hand, this suggests that the interaction of ParA and DivIVA inhibits cell elongation; on the other hand, it suggests that ParA binding to DivIVA promotes elongation. One possible explanation for this apparent inconsistency is that ParA stabilises DivIVA (or regulates its phosphorylation) and consequently enhances polar growth, while the absence of ParA promotes the relocation of DivIVA and the establishment of the new pole, increasing its elongation rate and also contributing to faster cell elongation. ParA could fulfil such a function, affecting the interplay between DivIVA and LamA or CswA. However, if interaction with ParA contributed to relocation of DivIVA, it would lead to a more symmetrical elongation of the strain with ParAT3A, and that was not observed (Fig. S6). An alternative explanation is that DivIVA activity is modified in different ways, depending on the nucleotide state of ParA; inactivated ParA-ADP released from the nucleoid after segregation (or ParA-ATP monomer, after nucleotide exchange) could inhibit cell elongation. In contrast, a ParA-ATP dimer (such as ParAR219E) recruited to DivIVA could modify its activity, increasing the rate of cell elongation. Finally, another explanation for the fast cell elongation rate caused by ParAT3A is that the release of nucleoid attachment to the pole increases polar growth. This phenomenon would mean that ParA, by interacting with DivIVA, enhances its activity but mediates nucleoid attachment at the old pole; however, pulling the nucleoid behind the pole slows cell extension. Further studies are required to test the above hypotheses and elucidate the mechanism by which DivIVA activity is regulated by ParA.

#### *Model of ParA-DivIVA interaction during the mycobacterial cell cycle*

To summarise, on the basis of our results, we propose a role for the ParA-DivIVA interaction in cell cycle coordination (Fig. 5). During chromosome segregation, the ParA-ADP dimer is released from the nucleoid after ATP hydrolysis induced by interaction with the ParB complex. At that time, ParA-ADP dimer is transiently recruited to the polar DivIVA complex. This interaction facilitates the formation of ParA gradient and movement of ParB complexes towards the new pole. The ParB complex moving towards the new pole rapidly migrates over the nucleoid according to a mechanism reminiscent of *C. crescentus* or *V. cholerae* unidirectional segregation. The

segregation of the ParB complex towards the old pole is not dependent on ParA-DNA interaction. However the precise positioning of the old pole ParB complex depends on ParA-DivIVA interaction. We suggest that the fast growth rate of the old pole requires the attachment of the nucleoid via the *oriC* region to prevent the chromosome from falling behind the pole and missegregating during cell division. However, the attachment of the nucleoid to the pole may slow its elongation rate. On the other hand, the transient accumulation of ParA at the poles affects DivIVA function by stimulating its activity in peptidoglycan synthesis or by modulating its stability and/or interaction with other protein(s). Thus the ParA-DivIVA interaction links chromosome segregation with cell extension.

## Experimental procedures

### *Cloning and E. coli growth conditions*

DNA manipulations were performed using standard protocols (Russell and Sambrook, 2001). Reagents and enzymes were supplied by Sigma-Aldrich, Roth and Thermo-Scientific. Oligonucleotides were synthesised by Sigma-Aldrich and Microsynth, and sequencing was performed by Microsynth and Genomed.

*E. coli* strains were grown in Luria-Bertani (LB) medium at 37°C (DH5 $\alpha$ , BL21(DE3)) or 30°C (BTH101). Culture conditions, antibiotic concentrations, and transformation protocols followed standard procedures (Russell and Sambrook, 2001).

### *E. coli interaction studies*

The plasmids used in bacterial two-hybrid (BTH) analyses are listed in Supplementary Table 1. BTH interaction studies were performed as previously described (Karimova *et al.*, 1998). The assays of  $\beta$ -galactosidase activity in liquid cultures were performed as described in the BACTH System Kit, Euromedex. Details of the *parA* mutant library construction in the pKT25 plasmid and its screening for ParA proteins that failed to interact with DivIVA are provided in the Supporting Information file. The cloning of the *M. smegmatis parA* gene into the BTH plasmids allowed the production of protein starting with the sequence MDTP, which is different from the sequence annotation in databases but, according to our earlier observation, corresponds to the N-terminus of the native protein. *E. coli* co-localisation assays are described in the Supporting Information.

### *Mycobacterium growth conditions*

The *M. smegmatis* strains used in this study are listed in Table S1. The construction of the *M. smegmatis* mutant strains is described in the Supporting Information. *M. smegmatis* strains were grown either in Middlebrook liquid 7H9 medium (Difco) supplemented with 10% OADC, (oleic acid-albumin-dextrose-catalase (BD)), and 0.05% Tween

80 or on solid 7H10 supplemented with 10% OADC, 0.5% glycerol and 0.05% Tween 80 unless otherwise stated. Mycobacterium growth assays

For most experiments, *M. smegmatis* strains from glycerol stocks were used to inoculate starting cultures, which were then grown for 24 h as a seed culture and used for the inoculation of precultures. After being incubated to log phase ( $OD_{600}$  0.5), the precultures were diluted in fresh medium to an  $OD_{600}$  of 0.05 and cultured to the desired OD.

For growth curve analyses, *M. smegmatis* strains were inoculated from glycerol stocks and grown to log phase ( $OD_{600}$  0.3–0.4). Next, the cultures were diluted in fresh medium to  $OD_{600}$  0.05, and 300  $\mu$ l of diluted culture was loaded into wells of a Bioscreen C-compatible honeycomb plate. The microplate cultures were incubated at 37°C with continuous shaking using Bioscreen C (Automated Growth Curves Analysis System, Growth Curves (Alab)), which allowed optical density measurements every 20 min.

### Fluorescence microscopy analysis of *M. smegmatis*

For snapshot microscopy, *M. smegmatis* strains were grown to mid-log phase ( $OD_{600}$  0.5) in 7H9 medium (as described above). For DNA staining, cells were treated with DAPI (2  $\mu$ g  $ml^{-1}$ ) for 2 h. After centrifugation (5000 rpm, 5 min), cells were resuspended in PBS, and clumps were disrupted by a vortex mixer. Bacteria were transferred to a glass slide with a 1% agarose pad soaked in 7H9 medium, covered with a coverslip or smeared on microscopic slides, dried and mounted with 5  $\mu$ l of PBS-glycerol (1:1) solution. Microscopy analysis was performed using a Zeiss Axio Imager Z1 equipped with a 100 $\times$  objective.

For time-lapse microscopy the experimental setup based on solid medium in an uncoated ibidi  $\mu$ -Dish (35 mm, low) was used. *M. smegmatis* strains were precultured as described above, and the de-clumped cell suspension was spread on solid 7H10 medium on an ibidi slide. For membrane staining, FM 5-95 (Thermo Fisher Scientific, Waltham, MA, USA) was added to 7H10 medium to a final concentration of 0.5  $\mu$ g  $ml^{-1}$ . Bacteria were imaged with a DeltaVision microscope (GE Healthcare, Chicago, IL, USA) equipped with 100 $\times$  and 60 $\times$  oil immersion objectives and an environmental chamber, which maintained a constant temperature of 37°C. Images were recorded every 10 min using differential interference contrast (DIC) and fluorescence channels (490/20 nm excitation filter and 528/38 nm emission filter for GFP and 575/25 nm excitation filter and 632/60 nm emission filter for mCherry) with a CoolSnap HQ2 camera. Images were processed with SoftWoRx software (GE Healthcare, Chicago, IL, USA).

Single-molecule-tracking photoactivated localisation microscopy (PALM) was performed using a custom-built total internal reflection fluorescence microscope, similar to a previously described procedure (Zawadzki *et al.*,

2015). Photoactivatable mCherry (PAmCherry) was activated with a 405 nm laser and then excited at 561 nm. To record bright-field cell images, an LED source and condenser (ASI Imaging) were used. Molecule tracking and localisation analysis were performed using custom-written MATLAB software (MathWorks, Natic, MA, USA). Bound and diffusing proteins were distinguished by calculating an apparent diffusion coefficient,  $D^* = MSD/(4 Dt)$ , from the mean-squared displacement (MSD) for each track with four steps. Due to cell confinement and motion blurring,  $D^*$  is an apparent diffusion coefficient (Stracy *et al.*, 2014). For structured illumination microscopy (SIM), an OMX V3 Blaze microscope (GE Healthcare, Chicago, IL, USA) equipped with a 60 $\times$ /1.42 oil UPlanSApo objective and 488 nm laser was used (Olympus, Shinjuku, Tokyo, Japan). Reconstruction of structured illumination (SI) raw data was performed with SoftWoRx 6.0 (GE Healthcare, Chicago, IL, USA) using a Wiener filter setting of 0.004. Reconstructed image stacks were visualised using SoftWoRx and ImageJ software. The fluorescence intensity along the cell was measured using the profile function of ImageJ software and R software.

### Acknowledgements

We would like to thank Jarno Makela for assistance with the PALM analysis and helpful discussion on the manuscript, Marc Bramkamp for critical reading of the manuscript and valuable comments, Grażyna Bieniarz for help with the BTH analysis and Agnieszka Strzałka for assisting with data analysis using the R statistical programming language. We are grateful to Jerod Ptacin and Lucy Shapiro for the kind gift of the pJP108 plasmid. This work was funded by Harmonia grant 2014/14/M/NZ1/00076 from the National Science Centre, Poland, which was awarded to DJ. KG acknowledges financial support from the Polish Ministry of Science and Higher Education 'Mobilnosc Plus' (1083/MOB/2013/0), and JZC acknowledges grant 2012/04/A/NZ1/00057 from the Maestro funding scheme, National Science Centre. The cost of publication was financed by the Wroclaw Centre of Biotechnology, programme of the Leading National Research Centre (KNOW) for years 2014–2018.

### Conflict of interests

The authors declare no competing interests.

### Author contributions

DJ and KG designed the research. TM, MM and IM prepared constructs with mutated *parA*. MP performed *E. coli* interaction analyses, constructed *M. smegmatis* strains and carried out their growth analyses. MP and DJ performed *M. smegmatis* microscopy analyses. KG, DT, DS and JZ-C helped with microscopy analyses and data interpretation. MP and DJ wrote the manuscript.

## References

- Aldridge, B.B., Fernandez-Suarez, M., Heller, D., Ambravaneswaran, V., Irimia, D., Toner, M., *et al.* (2012) Asymmetry and aging of mycobacterial cells lead to variable growth and antibiotic susceptibility. *Science*, **335**, 100–104.
- Badrinarayanan, A., Le, T.B.K. and Laub, M.T. (2015) Bacterial chromosome organization and segregation. *Annual Review of Cell and Developmental Biology*, **31**, 171–199.
- Bohm, K., Meyer, F., Rhomberg, A., Kalinowski, J., Donovan, C. and Bramkamp, M. (2017) Novel chromosome organization pattern in actinomycetales – overlapping replication cycles combined with diploidy. *MBio*, **8**, 1–18.
- Bowman, G.R., Comolli, L.R., Zhu, J., Eckart, M., Koenig, M., Downing, K.H., *et al.* (2008) A polymeric protein anchors the chromosomal origin/ParB complex at a bacterial cell pole. *Cell*, **134**, 945–955.
- Chaudhuri, B.N. and Dean, R. (2011) The evidence of large-scale DNA-induced compaction in the mycobacterial chromosomal ParB. *Journal of Molecular Biology*, **413**, 901–907.
- Ditkowski, B., Holmes, N., Rydzak, J., Donczew, M., Bezulska, M., Ginda, K., *et al.* (2013) Dynamic interplay of ParA with the polarity protein, Scy, coordinates the growth with chromosome segregation in *Streptomyces coelicolor*. *Open Biology*, **3**, 130006.
- Donczew, M., Mackiewicz, P., Wrobel, A., Flardh, K., Zakrzewska-Czerwińska, J., Jakimowicz, D., *et al.* (2016) ParA and ParB coordinate chromosome segregation with cell elongation and division during *Streptomyces* sporulation. *Open Biology*, **6**, 150263.
- Donovan, C. and Bramkamp, M. (2014) Cell division in *Corynebacterineae*. *Frontiers in Microbiology*, **5**, 132.
- Donovan, C., Schauss, A., Krämer, R. and Bramkamp, M. (2013) Chromosome segregation impacts on cell growth and division site selection in *Corynebacterium glutamicum*. *PLoS One*, **8**, e55078.
- Donovan, C., Sieger, B., Krämer, R. and Bramkamp, M. (2012) A synthetic *Escherichia coli* system identifies a conserved origin tethering factor in Actinobacteria. *Molecular Microbiology*, **84**, 105–116.
- Ebersbach, G., Briegel, A., Jensen, G.J. and Jacobs-Wagner, C. (2008) A self-associating protein critical for chromosome attachment, division, and polar organization in caulobacter. *Cell*, **134**, 956–968.
- Flårdh, K. (2003) Essential role of DivIVA in polar growth and morphogenesis in *Streptomyces coelicolor* A3(2). *Molecular Microbiology*, **49**, 1523–1536.
- Flårdh, K. (2010) Cell polarity and the control of apical growth in *Streptomyces*. *Current Opinion in Microbiology*, **13**, 758–765.
- Fogel, M.A. and Waldor, M.K. (2006) A dynamic, mitotic-like mechanism for bacterial chromosome segregation. *Genes & Development*, **20**, 3269–3282.
- Fung, E., Bouet, J.-Y. and Funnell, B.E. (2001) Probing the ATP-binding site of P1 ParA: partition and repression have different requirements for ATP binding and hydrolysis. *The EMBO Journal*, **20**, 4901–4911.
- Funnell, B.E. (2014) How to build segregation complexes in bacteria: use bridges. *Genes & Development*, **28**, 1140–1142.
- Le Gall, A., Cattoni, D.I., Guilhas, B., Mathieu-Demazière, C., Oudjedi, L., Fiche, J.-B., *et al.* (2016) Bacterial partition complexes segregate within the volume of the nucleoid. *Nature Communications*, **7**, 12107.
- Gerdes, K., Howard, M. and Szardenings, F. (2010) Pushing and pulling in prokaryotic DNA segregation. *Cell*, **141**, 927–942.
- Ginda, K., Bezulska, M., Ziółkiewicz, M., Dziadek, J., Zakrzewska-Czerwińska, J. and Jakimowicz, D. (2013) ParA of *Mycobacterium smegmatis* co-ordinates chromosome segregation with the cell cycle and interacts with the polar growth determinant DivIVA. *Molecular Microbiology*, **87**, 998–1012.
- Ginda, K., Santi, I., Bousbaine, D., Zakrzewska-Czerwińska, J., Jakimowicz, D. and McKinney, J. (2017) The studies of ParA and ParB dynamics reveal asymmetry of chromosome segregation in mycobacteria. *Molecular Microbiology*, **105**, 453–468.
- Graham, T.G.W., Wang, X., Song, D., Etson, C.M., van Oijen, A.M., Rudner, D.Z., *et al.* (2014) ParB spreading requires DNA bridging. *Genes & Development*, **28**, 1228–1238.
- Harms, A., Treuner-Lange, A., Schumacher, D. and Søgaard-Andersen, L. (2013) Tracking of chromosome and replisome dynamics in *Myxococcus xanthus* reveals a novel chromosome arrangement. *PLoS Genetics*, **9**, e1003802.
- Hester, C.M. and Lutkenhaus, J. (2007) Soj (ParA) DNA binding is mediated by conserved arginines and is essential for plasmid segregation. *Proceedings of the National Academy of Sciences*, **104**, 20326–20331.
- Hołówka, J., Trojanowski, D., Ginda, K., Wojtaś, B., Gielniewski, B., Jakimowicz, D., *et al.* (2017) HupB is a bacterial nucleoid-associated protein with an indispensable eukaryotic-like tail. *MBio*, **8**, e01272–17.
- Hołówka, J., Trojanowski, D., Janczak, M., Jakimowicz, D. and Zakrzewska-Czerwińska, J. (2018) The origin of chromosomal replication is asymmetrically positioned on the mycobacterial nucleoid and the timing of its firing depends on HupB. *Journal of Bacteriology*, **200**, 00044–18.
- Jakimowicz, D., Brzostek, A., Rumijowska-Galewicz, A., Zydek, P., Dołzbłasz, A., Smulczyk-Krawczyński, A., *et al.* (2007) Characterization of the mycobacterial chromosome segregation protein ParB and identification of its target in *Mycobacterium smegmatis*. *Microbiology*, **153**, 4050–4060.
- Jani, C., Eoh, H., Lee, J.J., Hamasha, K., Sahana, M.B., Han, J.-S., *et al.* (2010) Regulation of polar peptidoglycan biosynthesis by Wag31 phosphorylation in mycobacteria. *BMC Microbiology*, **10**, 327.
- Joyce, G., Williams, K.J., Robb, M., Noens, E., Tizzano, B., Shahrezaei, V., *et al.* (2012) Cell division site placement and asymmetric growth in mycobacteria. *PLoS One*, **7**, e44582.
- Kang, C.-M., Nyayapathy, S., Lee, J.-Y., Suh, J.-W. and Husson, R.N. (2008) Wag31, a homologue of the cell division protein DivIVA, regulates growth, morphology and polar cell wall synthesis in mycobacteria. *Microbiology*, **154**, 725–735.

- Kang, C., Abbott, D.W., Park, S.T., Dascher, C.C., Cantley, L.C. and Husson, R.N. (2005) The *Mycobacterium tuberculosis* serine/threonine kinases PknA and PknB: substrate identification and regulation of cell shape. *Genes & Development*, **19**, 1692–1704.
- Karimova, G., Pidoux, J., Ullmann, A. and Ladant, D. (1998) A bacterial two-hybrid system based on a reconstituted signal transduction pathway. *Proceedings of the National Academy of Sciences*, **95**, 5752–5756.
- Kiebusch, D., Michie, K.A., Essen, L.-O., Löwe, J., and Thanbichler, M. (2012) Localized dimerization and nucleoid binding drive gradient formation by the bacterial cell division inhibitor MipZ. *Molecular Cell*, **46**, 245–259.
- Kieser, K.J. and Rubin, E.J. (2014) How sisters grow apart: mycobacterial growth and division. *Nature Reviews Microbiology*, **12**, 550–562.
- Kleckner, N., Fisher, J.K., Stouf, M., White, M.A., Bates, D. and Witz, G. (2014) The bacterial nucleoid: nature, dynamics and sister segregation. *Current Opinion in Microbiology*, **22**, 127–137.
- Kloosterman, T.G., Lenarcic, R., Willis, C., Roberts, D.M. and Hamoen, L.W. (2016) Complex polar machinery required for proper chromosome segregation in vegetative and sporulating cells of *Bacillus subtilis*. *Molecular Microbiology*, **101**, 333–350.
- Kois-Ostrowska, A., Strzałka, A., Lipietta, N., Tilley, E., Zakrzewska-Czerwińska, J., Herron, P.R., *et al.* (2016) Unique function of the bacterial chromosome segregation machinery in apically growing *Streptomyces* – targeting the chromosome to new hyphal tubes and its anchorage at the tips. *PLOS Genetics*, **12**, e1006488.
- Leonard, T.A., Butler, P.J. and Lowe, J. (2005) Bacterial chromosome segregation: structure and DNA binding of the Soj dimer – a conserved biological switch. *The EMBO Journal*, **24**, 270–282.
- Letek, M., Fiuza, M., Villadangos, A.F., Mateos, L.M. and Gil, J.A. (2012) Cytoskeletal proteins of actinobacteria. *The International Journal of Biochemistry & Cell Biology*, **2012**, 905832.
- Lim, H.C., Surovtsev, I.V., Beltran, B.G., Huang, F., Bewersdorf, J. and Jacobs-Wagner, C. (2014) Evidence for a DNA-relay mechanism in ParABS-mediated chromosome segregation. *eLife*, **3**, e02758.
- Lin, L., Osorio Valeriano, M., Harms, A., Søgaard-Andersen, L. and Thanbichler, M. (2017) Bactofilin-mediated organization of the ParABS chromosome segregation system in *Myxococcus xanthus*. *Nature Communications*, **8**, 1817.
- Logsdon, M.M., Ho, P.Y., Papavinasasundaram, K., Richardson, K., Cokol, M., Sassetti, C.M., *et al.* (2017) A parallel adder coordinates mycobacterial cell-cycle progression and cell-size homeostasis in the context of asymmetric growth and organization. *Current Biology*, **27**, 3367–3374.e7.
- Lutkenhaus, J. (2012) The ParA/MinD family puts things in their place. *Trends in Microbiology*, **20**, 411–418.
- Meniche, X., Otten, R., Siegrist, M.S., Baer, C.E., Murphy, K.C. and Bertozzi, C.R. (2014) Subpolar addition of new cell wall is directed by DivIVA in mycobacteria. *Proceedings of the National Academy of Sciences*, **111**, E3243–E3251.
- Mohl, D.A. and Gober, J.W. (1997) Cell cycle – dependent polar localization of chromosome partitioning proteins in *Caulobacter crescentus*. *Cell*, **88**, 675–684.
- Murray, H. and Errington, J. (2008) Dynamic control of the DNA replication initiation protein DnaA by Soj/ParA. *Cell*, **135**, 74–84.
- Nguyen, L., Scherr, N., Gatfield, J., Walburger, A., Pieters, J. and Thompson, C.J. (2007) Antigen 84, an effector of pleiomorphism in *Mycobacterium smegmatis*. *Journal of Bacteriology*, **189**, 7896–7910.
- Plocinski, P., Arora, N., Sarva, K., Blaszczyk, E., Qin, H., Das, N., *et al.* (2012) *Mycobacterium tuberculosis* CwsA interacts with CrgA and Wag31, and the CrgA-CwsA complex is involved in peptidoglycan synthesis and cell shape determination. *Journal of Bacteriology*, **194**, 6398–6409.
- Plocinski, P., Martinez, L., Sarva, K., Plocinska, R., Madiraju, M. and Rajagopalan, M. (2013) *Mycobacterium tuberculosis* CwsA overproduction modulates cell division and cell wall synthesis. *Tuberculosis*, **93**, S21–S27.
- Priestman, M., Thomas, P., Robertson, B.D. and Shahrezaei, V. (2017) Mycobacteria modify their cell size control under sub-optimal carbon sources. *Frontiers in Cell and Developmental Biology*, **5**, 64.
- Ptacin, J.L., Gahlmann, A., Bowman, G.R., Perez, A.M., von Diezmann, A.R.S., Eckart, M.R., *et al.* (2014) Bacterial scaffold directs pole-specific centromere segregation. *Proceedings of the National Academy of Sciences*, **111**, E2046–2055.
- Ptacin, J.L., Lee, S.F., Garner, E.C., Toro, E., Eckart, M., Comolli, L.R., *et al.* (2010) A spindle-like apparatus guides bacterial chromosome segregation. *Nature Cell Biology*, **12**, 791–798.
- Rego, E.H., Audette, R.E. and Rubin, E.J. (2017) Deletion of a mycobacterial divisome factor collapses single-cell phenotypic heterogeneity. *Nature*, **546**, 153–157.
- Russell, D.W., and Sambrook, J. (2001) *Molecular Cloning: A Laboratory Manual*. Cold Spring Harbor, NY: Cold Spring Harbor Laboratory Press.
- Santi, I., Dhar, N., Bousbaine, D., Wakamoto, Y. and McKinney, J.D. (2013) Single-cell dynamics of the chromosome replication and cell division cycles in mycobacteria. *Nature Communications*, **4**, 2470.
- Schofield, W.B., Lim, H.C. and Jacobs-Wagner, C. (2010) Cell cycle coordination and regulation of bacterial chromosome segregation dynamics by polarly localized proteins. *The EMBO Journal*, **29**, 3068–3081.
- Singh, B., Nitharwal, R.G., Ramesh, M., Pettersson, B.M.F., Kirsebom, L.A. and Dasgupta, S. (2013) Asymmetric growth and division in *Mycobacterium spp.*: compensatory mechanisms for non-medial septa. *Molecular Microbiology*, **88**, 64–76.
- Stracy, M., Uphoff, S., Garza de Leon, F. and Kapanidis, A.N. (2014) In vivo single-molecule imaging of bacterial DNA replication, transcription, and repair. *FEBS Letters*, **588**, 3585–3594.
- Surovtsev, I.V., Campos, M. and Jacobs-Wagner, C. (2016) DNA-relay mechanism is sufficient to explain ParA-dependent intracellular transport and patterning of single and multiple cargos. *Proceedings of the National Academy of Sciences*, **113**, E7268–E7276.

- Toro, E., Hong, S., Mcadams, H.H. and Shapiro, L. (2008) Caulobacter requires a dedicated mechanism to initiate chromosome segregation. *Proceedings of the National Academy of Science*, **105**, 15435–15440.
- Treuner-Lange, A. and Sogaard-Andersen, L. (2014) Regulation of cell polarity in bacteria. *The Journal of Cell Biology*, **206**, 7–17.
- Trojanowski, D., Ginda, K., Pióro, M., Hołowka, J., Skut, P., Jakimowicz, D., *et al.* (2015) Choreography of the mycobacterium replication machinery during the cell cycle. *MBio*, **6**, e02125–14.
- Trojanowski, D., Hołowka, J., Ginda, K., Jakimowicz, D. and Zakrzewska-Czerwińska, J. (2017) Multifork chromosome replication in slow-growing bacteria. *Scientific Reports*, **7**, 43836.
- Uhía, I., Priestman, M., Joyce, G., Krishnan, N., Shahrezaei, V. and Robertson, B.D. (2018) Analysis of ParAB dynamics in mycobacteria shows active movement of ParB and differential inheritance of ParA. *PLoS One*, **13**, e0199316.
- Vecchiarelli, A.G., Neuman, K.C. and Mizuuchi, K. (2014) A propagating ATPase gradient drives transport of surface-confined cellular cargo. *Proceedings of the National Academy of Sciences*, **111**, 4880–4885.
- Wang, X., Montero Llopis, P. and Rudner, D.Z. (2013) Organization and segregation of bacterial chromosomes. *Nature Reviews Genetics*, **14**, 191–203.
- Wang, X., Montero Llopis, P. and Rudner, D.Z. (2014) *Bacillus subtilis* chromosome organization oscillates between two distinct patterns. *Proceedings of the National Academy of Sciences*, **111**, 12877–12882.
- Wu, L.J. and Errington, J. (2003) RacA and the Soj-Spo0J system combine to effect polar chromosome segregation in sporulating *Bacillus subtilis*. *Molecular Microbiology*, **49**, 1463–1475.
- Yamaichi, Y., Bruckner, R., Ringgaard, S., Möll, A., Ewen Cameron, D., Briegel, A., *et al.* (2012) A multidomain hub anchors the chromosome segregation and chemotactic machinery to the bacterial pole. *Genes & Development*, **26**, 2348–2360.
- Zawadzki, P., Stracy, M., Ginda, K., Zawadzka, K., Lesterlin, C., Kapanidis, A.N. and Sherratt, D.J. (2015) The localization and action of Topoisomerase IV in *Escherichia coli* chromosome segregation is coordinated by the SMC complex, MukBEF. *Cell Reports*, **13**, 2587–2596.
- Zhang, H. and Schumacher, M.A. (2017) Structures of partition protein ParA with nonspecific DNA and ParB effector reveal molecular insights into principles governing Walker-box DNA segregation. *Genes & Development*, **31**, 1–12.

### Supporting information

Additional supporting information may be found online in the Supporting Information section at the end of the article.